Full length article

# Best practices for autonomous measurement of seawater pH with the Honeywell Durafet

CrossMark

Philip J. Bresnahan Jr. [a], Todd R. Martz [a,*], Yuichiro Takeshita [a], Kenneth S. Johnson [b], Makaila LaShomb [a]

[a] Scripps Institution of Oceanography, University of California San Diego, 9500 Gilman Drive, La Jolla, CA 92093, USA
[b] Monterey Bay Aquarium Research Institute, 7700 Sandholdt Road, Moss Landing, CA 95039, USA

G R A P H I C A L   A B S T R A C T
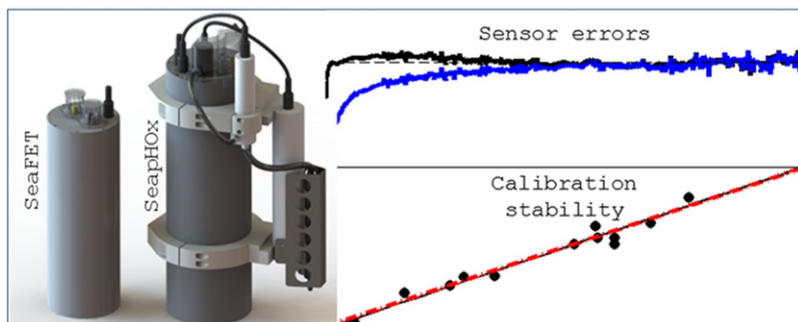
A R T I C L E   I N F O

A B S T R A C T

Performance of autonomous pH sensors is evaluated by comparing *in situ* data to independent bench-top measurements of pH and to co-located pH, O_2, and pCO_2 sensors. While the best practice is always to deploy a properly calibrated sensor, the lengthy time period required for sensor conditioning and calibration often results in sensor deployment without comprehensive calibration. Quality control (QC) procedures are examined to determine the errors

* Corresponding author. Tel.: +1 858 534 7466.
E-mail address: trmartz@ucsd.edu (T.R. Martz).

associated with different *in situ* calibration approaches and lay a framework for best practices. Sensor packages employing the Honeywell Durafet remained stable across multiple deployments for over nine months. However, sensor performance was often limited by biofouling. Regional empirical relationships for estimating carbonate system parameters are shown to enable identification of otherwise indistinguishable sensor offset and drift when multiple sensor types are co-located. Uncertainty is determined by calibration approach and must be quantified on a case-by-case basis. Our results indicate that the Durafet is capable of accuracy, relative to a chosen reference, of better than 0.03 pH units over multiple months. Accuracy is improved when a robust shore-side calibration is performed, an independent means of QC is available throughout a deployment, and effective biofouling prevention measures are taken.

1. Introduction

A recent trend in ocean acidification (OA) research involves utilizing natural settings in order to incorporate the variability inherent in nature (Hofmann et al., 2011; Kline et al., 2012). Although Standard Operating Procedures (SOPs) have been established for CO_2 bottle analyses (Dickson, 2007) and laboratory-based OA experiments (Riebesell et al., 2010), no standard protocols are in place for calibration and validation of the sensors used to characterize the natural settings of *in situ* experiments, despite their increasing prevalence (e.g. Byrne et al., 2009; Cullison Gray et al., 2011; Easley et al., 2013; Frieder et al., 2012; Liu et al., 2006; Martz et al., 2010; Seidel et al., 2008; Yu et al., 2011). In addition to OA studies, a number of equally important applications for quantitative biogeochemical studies exist for pH sensors (e.g. Emerson et al., 2011; Martz et al., 2014) that would benefit from documented validation and quality control (QC) protocols. Furthermore, pH measurements used to investigate specific processes – from climate trends to organismal responses – should always carry a statement of the uncertainty in the number reported. Establishing data QC protocols is of paramount importance and must be addressed before the relationship between observed pH and biogeochemical thresholds or biological "tipping points" is reported.

The initial accuracy of a stable sensor is limited by the calibration approach. Trust in pre- and post-calibrations (i.e., setting calibration constants before sensors are deployed or after they are recovered) of any marine chemical sensor relies on two hard to satisfy criteria: (1) sensors must be calibrated in a similar physical setting (*viz.*, similar temperature, salinity, pressure) to that of the study location and (2) sensors must not undergo significant (re)conditioning in their new environments. It is always preferred to rigorously calibrate a sensor before deployment, but this may require facilities and time that are not available. Honeywell provides an initial factory calibration of every Durafet sensor on the NBS pH scale, but provides no statement of calibration accuracy or stability, recommending that the user perform the canonical NBS buffer standardization employed widely for all glass electrodes. Because the NBS pH scale is not recommended for seawater pH measurements (Marion et al., 2011), at minimum, the Honeywell factory calibration must be recalibrated on the appropriate pH scale (e.g., the seawater scale, total hydrogen ion scale) before use in most oceanographic applications. Examples of such conversions are provided in the Supplementary data (see Appendix A). Due to these complications, it is sometimes preferred to calibrate an operating Durafet to a field measurement after the sensor is deployed. This practice also serves to validate laboratory calibration. Clearly, the calibration sample must coincide in time and space with a sensor measurement—a challenging demand in dynamic environments. Here, we evaluate the utility of *in situ* calibrations via bottle samples as well as independent, co-located sensors linked through regional empirical relationships.
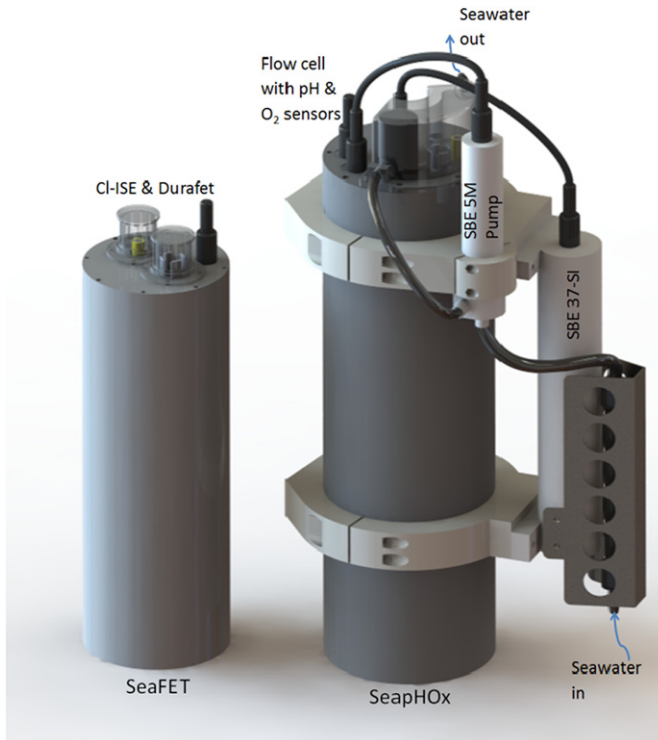
Fig. 1. SeaFET and SeapHOx sensor packages.

Specifically, we utilize the relationships derived by Alin et al. (2012) who report estimates for marine inorganic carbon parameters below the mixed layer in the CalCOFI Sampling Region ($27°N$–$37°N$) based on oxygen, temperature, salinity, and density.

While a sensor with a self-calibrating mechanism is desirable for obvious reasons, such systems are quite rare due to the complexity of automating the calibration process. The MAPCO$_2$ is currently the only sensor capable of measuring a CO$_2$ system variable with self-calibration (Friederich et al., 1995). The Durafet's demonstrated stability and longevity (Martz et al., 2010, present study) warrant its continued use without self-calibration capability and heeding the recommendations set forth here will likely augment data quality for the Durafet and other systems with no self-calibration. Based on a number of deployment examples, we outline a set of best practices that we have found useful for rejecting bad data and estimating uncertainty. The analysis techniques and recommendations described will prove helpful for the ocean chemical sensor community at large and Durafet sensor users in particular.

2. Materials and methods

2.1. Sensors

Ion Sensitive Field Effect Transistor (ISFET) pH sensors used in this work were deployed in a variety of configurations. The "SeaFET" design consists of a Honeywell Durafet and a solid-state chloride ion selective electrode (Cl-ISE) (Martz et al., 2010) whereas the "SeapHOx" is an integrated sensor package consisting of a Durafet, Cl-ISE, oxygen sensor (Aanderaa Data Instruments 3835 Optode), and a conductivity-temperature sensor (Sea-Bird Electronics SBE 37), all plumbed into a pumped flow stream (Fig. 1). The SeaFET has been commercialized by Satlantic, L.P.

Unlike potentiometric glass electrodes, the ISFET sensor is an active electronic device, based on Metal Oxide Semiconductor Field Effect Transistor (MOSFET) technology. When exposed to solution, the oxide coating of the MOSFET's conduction channel exchanges protons, giving rise to an interface potential that is measured as a voltage between the source of the MOSFET and a reference electrode. For further details the reader is referred to Bergveld (2003). In both the SeaFET and SeapHOx, the ISFET voltage is recorded relative to two independent reference electrodes: an *internal* Ag/AgCl reference with a liquid junction and a junctionless *external* Cl-ISE, referred to hereafter as E_{INT} and E_{EXT}, respectively (Martz et al., 2010).

Nominal voltage ranges in seawater are $E_{INT} \approx 0.03$ to 0.1 V, $E_{EXT} \approx -0.95$ to -0.8 V. Corresponding pH^{INT} and pH^{EXT} values are derived from E_{INT} and E_{EXT}, respectively. The dual reference electrode design is not a requirement. Due to the classic difficulty of achieving a stable potentiometric reference (Culberson, 1981), we elected to build a system with two independent reference electrodes (Martz et al., 2010). In our opinion, the external reference provides a theoretical improvement due to the fact that the liquid junction potential of the internal reference is unquantifiable and therefore adds uncertainty to the pH^{INT} value. However, we have also found by experience that the internal reference electrode is of the highest quality and, under many circumstances, appears to remain nearly as stable as the external reference. Retaining two reference electrodes thus provides a simple check during data QC: differences between pH^{INT} and pH^{EXT} serve as an indicator of sensor malfunction or fouling.

The approach to biofouling prevention has evolved along with our continued implementation of the *in situ* Durafet sensor. SeaFET biofouling prevention is passive: seawater is exchanged across a copper mesh screen enclosing the sensors. Improvements to the original SeaFET design include the incorporation of a flow cell over the sensors and inclusion of 70:30 Cu–Ni alloy tubing, which has proven superior to the original Cu mesh. SeaFET data discussed herein utilize the former design with Cu mesh screen. The pumped flow circuit of the SeapHOx takes advantage of the tributyltin biocide plugs located at the inlet and outlet of the conductivity cell of the SBE 37. The enclosures for both packages block most light, reducing biofouling and mitigating the direct impact of light on sensor response, which can be substantial for an ISFET. See Supplementary data (Appendix A) for further discussion of biofouling.

2.2. pH calculation

In the following section, we lay out the derivation of equations necessary for calculation of pH and calibration constants relative to both reference electrodes from sensor voltages, temperature, and salinity. For the proton-sensitive ISFET and chloride-sensitive reference electrodes, the Nernst equation gives

$$E = E^* - S \times \log(a_H a_{Cl}), \quad \text{where} \tag{1}$$

$$S = \frac{RT}{F} \times \ln 10, \quad \text{and} \tag{2}$$

$$\log(a_H a_{Cl}) = \log(\gamma_H \gamma_{Cl}) + \log(m_H m_{Cl}) = \log(\gamma_H \gamma_{Cl} m_{Cl}) - pH. \tag{3}$$

E is the measured sensor voltage, $R = 8.3145$ Jmol^{-1}K^{-1}, $F = 96, 487$ Cmol^{-1}, T is temperature in Kelvin, and a_H and a_{Cl} are the proton and chloride ion activities. γ and m represent activity coefficients and molality, respectively. Note that with the exception of the calculation of the Nernst slope, S, hereafter T represents °C.

Rearranging Eq. (1) to solve for the calibration constant, E^*, and inserting the right-hand side of Eq. (3) yields

$$E^* = E + S \times [\log(\gamma_H \gamma_{Cl} m_{Cl}) - pH]. \tag{4}$$

Here we begin distinguishing between internal and external values. In solving for E^*_{INT}, we group $\{E^* - S \times [\log(\gamma_H \gamma_{Cl} m_{Cl})]\}$ in Eq. (4) and rename this term E^*_{INT} such that

$$E^*_{INT}(T) = E_{INT}(T) - S(T) \times pH_{tot}(T); \tag{5}$$

$$E^*_{INT,25} = E^*_{INT}(T = 25\,°C) = E^*_{INT}(T) + \frac{dE^*_{INT}}{dT}(25\,°C - T). \tag{6}$$

E_{EXT} responds to the activity of HCl, a_{HCl}, in seawater. In order to account for the changing chloride ion concentration and activity coefficients due to varying environmental conditions (*e.g.*, temperature and salinity), we calculate $\log(\gamma_H \gamma_{Cl} m_{Cl})$ explicitly (Dickson, 2007; Khoo et al., 1977) and combine this with pH on the free hydrogen ion concentration scale:

$$E^*_{EXT}(T) = E_{EXT}(T) + S \times \log(\gamma_H \gamma_{Cl} m_{Cl}) - S \times pH_{free}; \tag{7}$$

$$E^*_{EXT,25} = E^*_{EXT}(T = 25\,^\circ C) = E^*_{EXT}(T) + \frac{dE^*_{EXT}}{dT}(25\,^\circ C - T). \tag{8}$$

$E_{INT}(T)$, $E_{EXT}(T)$, and pH(T) are the recorded voltage and pH at the calibration point. Our standard practice involves transforming the pH_{free} derived from E_{EXT} to pH_{tot} as a final step during data processing, in order to compare pH^{EXT} to pH^{INT}. A Matlab script to calibrate the Durafet and calculate pH from recorded voltages, temperature, and salinity is provided in Supplementary data (see Appendix A).

2.3. Calibration

Experience indicates that the Durafet and Cl-ISE remain stable over multiple months when deployed continuously in seawater. Subsequent work, including this study, establishes that (1) the Durafet sensors repeatedly demonstrate a 100% Nernstian response (Takeshita et al., submitted for publication) and (2) exhibit a stable and repeatable potential at a given temperature, salinity, and pH, with a highly linear and stable response to temperature. Across multiple sensors, the reference potential at a given temperature (e.g., 25 °C: E^*_{25}), is expected to vary by $\sim$ 1% and the temperature coefficient dE^*/dT by $\sim$ 10% (Martz et al., 2010). A 10% difference in dE^*/dT introduces errors of <0.015 pH over the temperature range observed in these studies; therefore, an average dE^*/dT is used for all sensors (values are reported by Martz et al. (2010)). The findings of Martz et al. (2010) and data below demonstrating long-term sensor stability justify a single-point calibration approach under most circumstances. The Durafet's highest achievable accuracy (better than 0.01) may require analysis of the value and stability of dE^*/dT for individual sensors.

The single-point calibration, specific to each reference electrode, defines the intercept (E^*) in a line of pH vs. sensor voltage (E) at *in situ* calibration conditions (Eq. (4) for general case; 5 and 7 for internal and external references, respectively). The calibration point is thus specified as a sensor voltage at a particular pH, temperature, and salinity; sensor voltages are extended over a range of pH, temperature, and salinity by assuming a 100% Nernst slope and a constant dE^*/dT. Due to the inter-sensor variability, E^*, corrected to a standard temperature, is described better as a "calibration constant" than as a "standard potential". It is essential to note that while pH calibration is carried out on the total scale for E^*_{INT}, it *must* be carried out on the free scale for E^*_{EXT} as the free proton concentration must be known to calculate the logarithm term in Eq. (7). For a thorough description of the various pH scales and inter-conversions, the reader is referred to Marion et al. (2011).

2.4. Characteristic electrode responses

As discussed by Martz et al. (2010) the external reference electrode exhibits a sensitive yet predictable response to salinity while the internal reference responds little to salinity over the ranges observed in this study (32.8–34.2 on the practical salinity scale (PSS-78) in oceanic deployments). Due to the unmeasurable liquid junction potential, pH^{INT} has a poorly characterized (yet small) salinity response that leads to increasing errors as salinity departs from that at the time of calibration. Although this error in pH^{INT} is presumed to be small over narrow salinity ranges, this may not be the case during large salinity variations. The thermodynamic uncertainty due to the liquid junction potential cannot be ignored when the sensor is deployed in coastal locations with significant freshwater input or large temperature variability. However, in test tank experiments over the salinity range 30–36, we are unable to identify an effect on the liquid junction potential and therefore recommend no salinity correction for the pH^{INT} under typical seawater conditions, as described in Results and discussion. Upon first contact with seawater, pH sensor voltages relative to both reference electrodes exhibit an asymptotic drift. This conditioning period arises from several sources: (1) achieving a stable flow of ions across

the liquid junction of the internal reference electrode (nominally hours), (2) replacement of Cl^- with Br^- in the solid solution of AgCl of the Cl-ISE (nominally days), (3) an ISFET conditioning component, related to the initial power-up of the chip, the exact basis of which is not fully understood (nominally 1 day), and (4) a pressure effect on the ISFET and internal reference electrode through changes in the liquid junction potential that may become important if the sensor is deployed more than $\sim$20 m below the surface (nominally 1 h). Factors 1–3 can be addressed by operating the pH sensor continuously in seawater (never powering off the ISFET) for one week prior to deployment and taking care to keep the sensor wetted in natural seawater during transport. Unfortunately, as discussed below, these preconditioning procedures are often ignored due to the time constraints of the deployment window, resulting in sensor drift during the first days of a deployment. The fourth aspect of conditioning (a pressure effect) is problematic to characterize as it appears to be sensor specific and not necessarily repeatable. Using the Durafet sensor for profiling applications in the 0–80 m range (rated depth) is therefore discouraged. However, as shown here, Durafets have been successfully operated beyond 80 m; the key to a successful deployment rests in selecting an appropriate reference pH once the sensor is deployed and conditioned at depth.

2.5. Ancillary data

Prior to deployment, Aanderaa optodes underwent a two-point correction (zero and atmospheric saturation), in accordance with the manufacturer's recommendations, to account for changes in the factory calibration. The surface $p\text{CO}_2$ measurements made by the PMEL MAPCO$_2$ systems were calibrated using span gases to achieve accuracy of better than 5 μatm (Friederich et al., 1995).

pH sensor measurements are compared to (1) measurements carried out on discrete samples, pH^{disc}, using standard bench top procedures (Dickson, 2007), (2) other co-located pH sensors and analyzers, and (3) other co-located chemical sensors used to derive empirical pH values with the regional relationships from Alin et al. (2012) and thermodynamic equations from the program CO2SYS for Matlab (Van Heuven et al., 2011). The pH estimated from observed oxygen and temperature ($\text{pH}_{\text{O}_2}^{\text{est}} = \text{pH}(\text{O}_2, T)$) is reported to have a root mean squared error of 0.024 pH units relative to measurements made using bottle samples in the 2005–2011 NACP West Coast Cruise dataset (Alin et al., 2012). $\text{pH}_{\text{O}_2}^{\text{est}}$ is therefore only calculated in the region delineated by that work. $TA^{\text{est}} = TA(T, S)$ is also calculated using the regional relationships from Alin et al. (2012) and, where $p\text{CO}_2$ data were available (from a PMEL MAPCO$_2$ sensor), they are combined to calculate $\text{pH}_{p\text{CO}_2}^{\text{est}} = \text{pH}(p\text{CO}_2, TA^{\text{est}})$. Combining the error in TA^{est} (6.4 μmolkg^{-1}) and $p\text{CO}_2$ (less than 5 μatm), we estimate a propagated error of less than 0.01 pH units using CO2SYS.

pH anomalies are reported as ΔpH^{i-j} where i and j refer to the pH terms described above (e.g., $\Delta\text{pH}^{\text{INT}-\text{disc}} = \text{pH}^{\text{INT}} - \text{pH}^{\text{disc}}$). Sensor offset (i.e., intercept), c_0, and slope, c_1, relative to a reference pH value (pH^{disc}, $\text{pH}_{\text{O}_2}^{\text{est}}$, or $\text{pH}_{p\text{CO}_2}^{\text{est}}$) are calculated from a Model II least squares fit (Peltzer, 2007) of property–property plots (namely, $\text{pH}^{\text{sensor}}$ vs. $\text{pH}^{\text{reference}}$).

2.6. Study sites

Data are presented from deployments under controlled laboratory conditions and at three field sites, each selected based on the availability of an independent validation approach (Table 1).

A SeaFET was co-located with an SBE-16 CTD and an Aanderaa optode in two consecutive mooring deployments (total sampling period of eighteen months) at 88 m on the Del Mar Buoy. The only configuration change between deployments was the refilling of the Durafet's internal reference electrolyte gel and replacement of the ceramic frit liquid junction. During this time, the 88 m sensors remained continuously beneath the surface mixed layer, providing an excellent setting in which to evaluate the empirical relationship for $\text{pH}_{\text{O}_2}^{\text{est}}$. In addition, four standard ship-based hydrocasts were carried out in close proximity to the 88 m sensors.

Seawater tanks at Scripps Institution of Oceanography were used to capture the conditioning process of two SeapHOx sensors. The conditioning experiment consisted of a 20 day deployment of new, unconditioned sensors in a 6000 L tank of seawater that had been previously filtered and then

Table 1
Deployment details.

Site	Regime	Lat. (°N)	Lon. (°W)	Sensor depth (m)	Bottom depth (m)	Sensor package(s)	Validation approach(es)
Del Mar Buoy (DMB, U. Send, SIO)	Near-shore	32.93	117.32	88	100	SeaFET, Optode, CTD	4 discrete samples, $pH_{O_2}^{est}$
Scripps Test Tank (SIO)	Laboratory	32.87	117.25	1	1	SeapHOx	Continuous spectrophotometric pH
Monterey Bay (L20, MBARI)	Near-shore	36.81	121.83	1	19	1 MBARI Durafet (also referred to as SeaFET0), 2 SeaFETs, 1 SeapHOx, 1 SAMI-pH	13 discrete samples, co-located pH sensors
California Current Ecosystem (CCE-2, U. Send, SIO)	Coastal Upwelling	34.32	120.82	1	770	SeapHOx, MAPCO2	$pH_{pCO_2}^{est}$
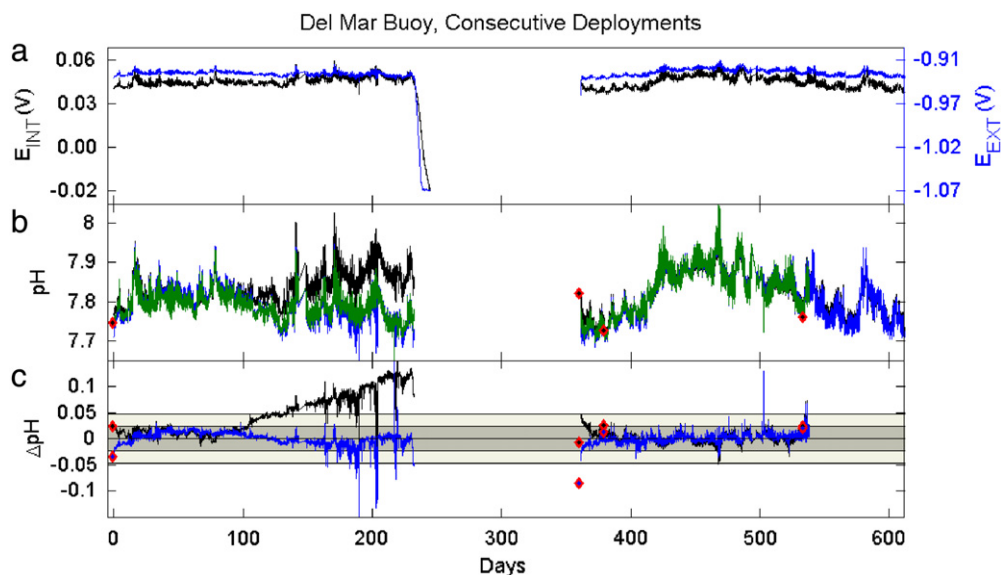
Fig. 2. Del Mar Buoy pH time-series beginning on 25-Jun-2011. (a) Raw sensor voltages for internal (black) and external (blue) reference electrodes show two consecutive deployments with a four-month gap. (b) pH is calculated using the internal and external reference electrodes and estimated from oxygen and temperature ($pH_{O_2}^{est}$, green). Discrete sample values are black diamonds with red edges. (c) Anomalies for pH^{INT} (black) and pH^{EXT} (blue) are shown relative to $pH_{O_2}^{est}$ (solid lines) and discrete samples (filled diamonds, red edges) with σ (dark gray) and 2σ (light gray) shaded regions, where standard error in $pH_{O_2}^{est}$ as reported by Alin et al. (2012) is 0.024 pH units. The optode failed on 15-Dec-2012 but the SeaFET functioned until 28-Feb-2013, leaving the pH time-series without a $pH_{O_2}^{est}$ value for the last 75 days. (For interpretation of the references to color in this figure legend, the reader is referred to the web version of this article.)

sterilized by ozonation. An automated spectrophotometric pH analyzer continuously measured pH on the tank water while the sensors were deployed. The effect of salinity on pH^{INT} and pH^{EXT} was assessed by diluting test tank salinity through discrete fresh water additions; finally, two SeapHOx packages were pressurized to discern the pressure effects on the Durafet and ISE.

The L20 mooring in Monterey Bay, CA, operated from July 12 to November 2, 2010, providing nearly four months of continuous sensor data from five independent pH sensors (Figure S1). Thirteen discrete bottle samples were collected using a 1 L bottle from a small boat during this period. Bottles were transported unpoisoned to the lab where pH was measured within 1 h. pH^{disc} was calculated from spectrophotometric pH (Clayton and Byrne, 1993) at 20°C and adjusted to *in situ* temperature using a constant slope of -0.015 pH°C^{-1}. Uncertainty in pH is dominated by use of unpurified pH indicator dye, which may result in errors up to 0.02 (Liu et al., 2011).

At the California Current Ecosystem coastal upwelling mooring (CCE-2) 1 m site, in addition to the SeapHOx, a PMEL MAPCO$_2$ sensor measured pCO_2. Here we employ empirical and thermodynamic relationships to calculate $pH_{pCO_2}^{est}$. The CCE moorings offer a rare opportunity to compare several co-located chemical sensors in a well-characterized region of the coastal ocean, significantly improving the ability to QC sensor data.

3. Results and discussion

3.1. Del Mar Buoy

The DMB data (Fig. 2) illustrate a complete cycle of sensor conditioning, drift, failure, maintenance, and redeployment. The SeaFET failure on 13-Feb-2012 (day 230) due to exhaustion of the battery pack is easily identified by examination of the raw sensor voltage (Fig. 2(a)). Upon deployment, a discrete

bottle sample was captured at 88 m from a rosette cast approximately 100 m away from the mooring and several hours after the sensor was situated at 88 m depth. Due to the lack of pre-conditioning for this particular sensor, the discrete sample could not be used as a calibration point. Upon examination of the pH values (Fig. 2(b)), it is evident that one or both of the pH signals began to drift around day 100 of the deployment. Anomalies relative to $pH_{O_2}^{est}$ (Fig. 2(c)) were minimized by setting E^* between days 20 and 50 of the deployment (after electrode conditioning and before the onset of detectable drift). These results strongly suggest a drift in the internal reference electrode.

The mooring was recovered on 25-May-2012 (day 332). The SeaFET electrodes were cleaned, including replacement of the Durafet's internal reference electrolyte gel and liquid junction, and the sensor was stored in air until redeployment on 24-Jun-2012. E^* values derived in the first deployment were applied to the redeployed SeaFET without adjustment. As seen in the right-hand portion of the time-series (Fig. 2(b), (c)), the pH calibration derived several months earlier held to better than 0.01 pH units (standard deviation of the anomaly time-series around an average anomaly of 0.002) for both reference electrodes throughout the second deployment. This result justifies the recommendation to define (and leave unchanged) E^* following a careful shoreside calibration (i.e., after the conditioning period). While in this particular case (that is, the DMB deployment), the calibration constants were calculated during deployment, by extension, this finding applies to pre-deployment calibrations, particularly since this sensor was returned to shore and then redeployed and shown to exhibit no bias. The drift observed in pH^{INT} during the first deployment of this sensor is attributed to the depletion of the internal electrolyte gel, or possibly a blockage of the liquid junction, as surmised from the sensor's return to a near-zero anomaly in the second deployment after replacement of the reference gel and liquid junction.
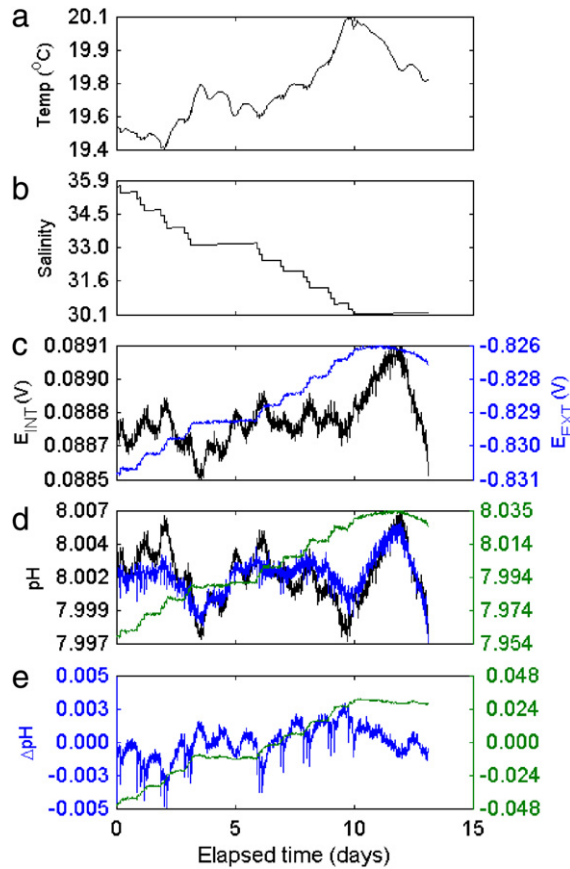
3.2. Scripps Test Tank

3.2.1. Salinity effect

In Fig. 3, we see the effect of rapidly changing salinity. The SeapHOx electrodes used in this experiment had already been conditioned. The spectrophotometric pH analyzer malfunctioned during this experiment, precluding the calculation of anomalies relative to an independent stable reference pH value. pH^{INT} and pH^{EXT} calculated using recorded salinity track each other closely in the long term (days) with a maximum anomaly magnitude of 0.005. This result is promising, demonstrating that the reference electrodes recondition similarly to new salinity. However, on the short term (minutes), there is a differing response time between the two calculated pH values that is exposed in sharp downward spikes in the $\Delta pH^{EXT-INT}$ anomaly time-series (Fig. 3(e) blue) that line up with the small step changes in salinity (Fig. 3(b)). Closer examination of the time-series suggests that these spikes are present in pH^{EXT}, not pH^{INT} and, furthermore, that they do not appear in the E_{EXT} time-series (Fig. 3(c)).

As the spikes are only present in calculated pH^{EXT} and not E_{EXT}, these larger anomalies must come from the dependence of pH^{EXT} on salinity, suggesting that the SeapHOx flow cell was not fully flushed in a single pumping cycle. This conclusion comes about from the observation that, for qualitatively smooth step changes in both salinity and E_{EXT}, the only remaining cause of spikiness in pH^{EXT} is effectively a true chemical mismatch between the water that the easily flushed conductivity-temperature sensor sampled and that which the more slowly flushed flow-cell-contained sensors (Durafet, ISE, and optode) sampled. In other words, the conductivity-temperature sensor sampled "new" seawater after the first pump cycle when fresh water was mixed into the tank but the pH sensor flow cell still contained seawater from the previous sample. The solution to this operational problem is a higher flush volume (achieved through longer pumping time and/or higher flow rate—engineering issues that have been addressed in the SeapHOx configuration). Importantly, the fact that these spikes result from configuration issues and not kinetic differences in electrode response times suggests that the spikes can be ignored insofar as chemical responses are concerned, making the $\Delta pH^{EXT-INT}$ anomaly negligible relative to calibration accuracy.

The anomaly based on calculation of pH using the experiment's average salinity (Fig. 3(e), green), increases by an order of magnitude, perhaps an obvious effect since pH^{EXT} is a function of salinity while

Fig. 3. The salinity of the Scripps Test Tank was changed from 35.9 to 30.1 by adding batches of fresh water at multiple intervals over fourteen days. Panels (a) and (b) show temperature and salinity, respectively. Panel (c) shows recorded E^{INT} and E^{EXT}. The left y-axis of panel (d) shows pH^{INT} (black) and pH^{EXT} (blue) calculated using the recorded salinity; the right axis shows pH^{EXT} (green) recalculated using the experiment's average salinity of 32.3. Panel (e) illustrates pH anomalies of $\Delta pH^{EXT-INT}$ (left axis, blue) using the recorded salinity in the calculation of pH^{EXT}; $\Delta pH^{EXT-INT}$ is shown (right axis, green) using the average salinity in the calculation of pH^{EXT}. (For interpretation of the references to color in this figure legend, the reader is referred to the web version of this article.)

pH^{INT} is not. The anomaly resulting from calculation of pH^{EXT} using an average salinity reinforces the need to deploy Durafet sensors with conductivity-temperature sensors. Because sensor performance has not been evaluated below $S = 30$ we are unable to provide recommendations for operating the sensor at lower salinities.

3.2.2. Pressure effect

Two SeapHOx sensors were pressurized from 0 to 35 dbar at the Scripps Test Tank Facility (Fig. 4). Pressure is shown to have the same first-order effect on all pH sensors tested: increasing pressure results in a decreasing pH signal. However, each sensor and reference electrode behaves slightly differently. *In situ* pH demonstrates that the effect of pressure on the carbonate system equilibrium constants is insufficient to account for the observed changes in sensor pH. We avoid publishing pressure coefficients for the Durafet and ISE because the effect of pressure is strongly sensor dependent (ISFET and/or reference electrodes), and a clear sign of hysteresis is observed. We therefore discourage profiling applications with the Durafet sensor packages, as noted in Materials and methods.
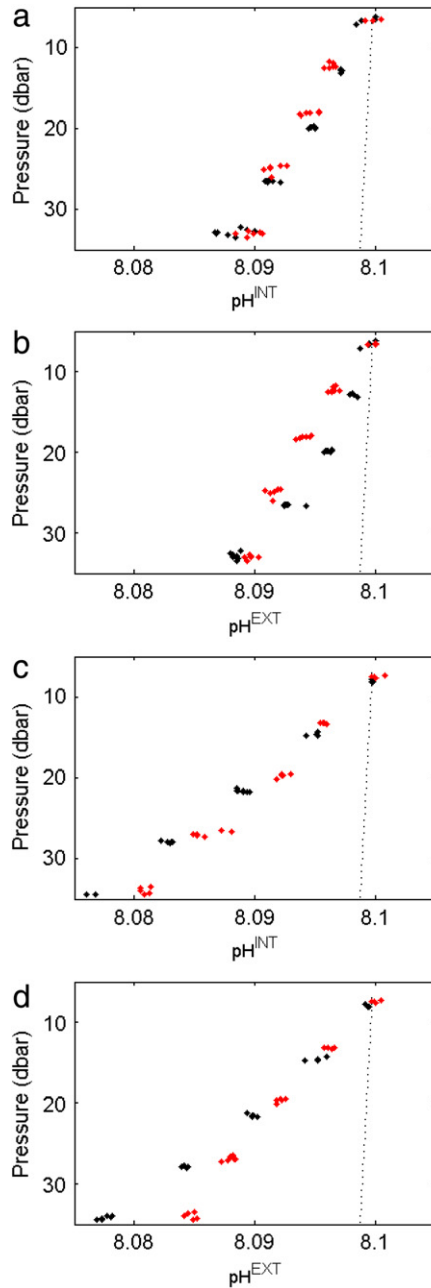
Fig. 4. Effect of pressurizing two SeapHOx sensor packages (SP041 (a, b) and SP040 (c, d)). Calculated sensor pH from increasing and decreasing pressure are shown as red and black dots, respectively. The in situ pH, calculated assuming constant TA and DIC, is represented by the black dotted lines.

3.2.3. Electrode conditioning

Fig. 5(a) clearly illustrates the sensor conditioning period. E^* was calculated using a spectrophotometric pH value at the end of the time-series. While the anomaly between pH^{INT} and
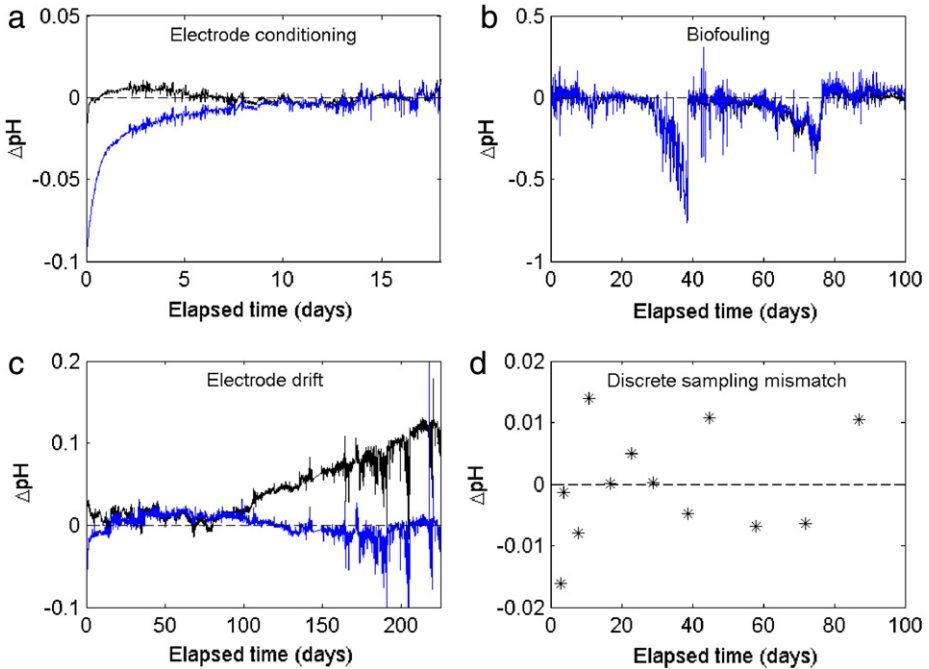
Fig. 5. Composite of anomaly time-series from (a) Scripps Test Tank SeapHOx, (b) L20 Mooring SeaFET2, (c) Del Mar Buoy SeaFET, and (d) L20 Mooring SeapHOx. Black and blue represent $\Delta pH^{INT-ref}$ and $\Delta pH^{EXT-ref}$, respectively. Reference pH values are (a) spectrophotometric, (b) pH^{INT} from a stable SeapHOx, (c) $pH_{O_2}^{est}$, and (d) discrete sample values. Black dashed lines represent a zero anomaly. Note that y-axis limits differ among the four deployments, indicating that there can be significant differences in the magnitudes of various errors. (For interpretation of the references to color in this figure legend, the reader is referred to the web version of this article.)

spectrophotometric pH very quickly approaches zero at the beginning of the deployment (several hour warm-up period), pH^{EXT} takes substantially longer (approximately eight days) to condition. This anomaly is not an issue once reference electrodes are conditioned to seawater, or more specifically, its bromide concentration.

3.3. MBARI L20

Results from the L20 deployment are shown in Figs. 5(b) and 6(a). No detectable drift was observed in the SeapHOx pH^{INT} relative to the discrete samples, within the sampling error. Accordingly, the SeapHOx pH^{INT} was calibrated to minimize the anomaly relative to discrete samples; that is, E^* was adjusted to force the mean $\Delta pH^{sensor-disc}$ to zero. All SeaFETs were calibrated to minimize their mean anomaly relative to SeapHOx pH^{INT} for the first five days of the deployment, before the onset of any detectable sensor drift. The resulting time-series from only one SeaFET is shown here, but all SeaFETs responded similarly, with biofouling dominating the anomaly signal on the week to month time scale (Figure S1). The L20 data illustrate how discrepancies can arise when calibrating to individual discrete samples. The time-series anomaly shown in Fig. 5(d) depicts the offset between sensor and discrete sample values that results when E^* is set using an average value to minimize the $\Delta pH^{INT-disc}$ anomaly. This anomaly results from: (1) significant environmental pH gradients combined with small spatiotemporal mismatch between sensor and discrete sample and/or (2) errors in the discrete sample analysis. Closer analysis of the L20 time-series (Supplementary data, Appendix A) suggests that spatiotemporal mismatch is the dominant control; in a dynamic near-shore ecosystem, a small sampling discrepancy could certainly contribute (unbiased) anomalies of this magnitude. By choosing a single calibration constant based on multiple discrete samples, the error is substantially reduced.
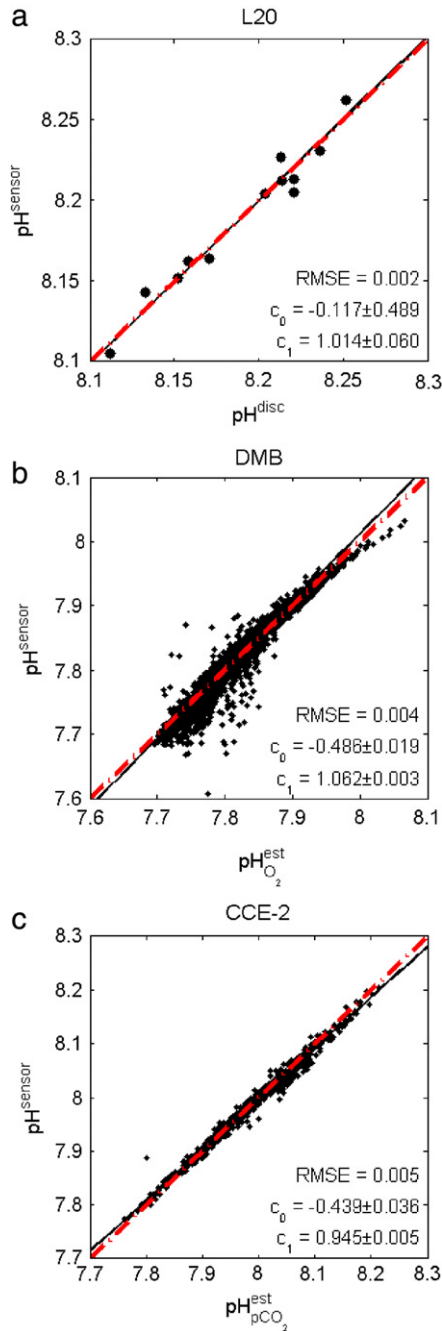
Fig. 6. Property–property plots of sensor pH vs. an independently measured (a) or estimated (b, c) reference pH. Data come from the (a) L20 deployment pH^{INT} vs. discrete sample pH, (b) Del Mar Buoy 88 m pH^{EXT} vs. $pH^{est}_{O_2}$, and (c) CCE-2 surface pH^{INT} vs. $pH^{est}_{pCO_2}$. Dashed red lines represent 1:1 ($pH^{sensor} = pH^{ref}$) and solid black lines are Model II least squares fits. In each plot, only one (stable) sensor pH is chosen. L20 (a) pH^{EXT} and DMB (b) pH^{INT} are not displayed here due to inaccuracies described in the text. CCE-2 (c) pH^{EXT} is not shown in order to simplify figure but agree closely with pH^{INT}.

3.4. California Current Ecosystem mooring: CCE-2

Several independent pH measurement techniques were employed at the CCE-2 1 m location, allowing a robust cross-comparison. Fig. 6(c) displays the property–property relationship between sensor pH^{INT} and $pH^{est}_{pCO_2}$, emphasizing the value of using an independent analyzer for an additional CO_2 system master variable. The SeapHOx calibration point was chosen to minimize the anomaly relative to $pH^{est}_{pCO_2}$, which is based on the internally-calibrated MAPCO$_2$ sensor.

3.5. Quality control

Our results demonstrate a critical dependence of sensor accuracy on choice of QC technique employed. In physically and biogeochemically dynamic environments, where it is challenging to capture synchronized discrete samples, alternate methods have been observed to disagree by greater than 0.1 pH units. At L20, SeapHOx sensors observed average pH changes of 0.023 pH · hr^{-1} but recorded instantaneous rates at least a full order of magnitude greater; calibrating to a sample with even slight spatiotemporal mismatch in such an environment can introduce significant errors. Moreover, the random anomalies in Fig. 5(d) suggests that resetting the calibration constant to match each discrete value would impart an artificial variability in calculated pH with a magnitude of ∼0.015 pH units and a frequency equal to the discrete sampling frequency. The recommendation to use an unchanging calibration for a given sensor is further supported by the DMB deployments, throughout which E^* is unchanged while results converge to near-zero anomalies following redeployment. These deployments suggest that, often, the electrode calibration constant remains stable and the pH anomaly arises from sampling mismatch. In summary, we recommend first eliminating sensor data with identifiable drift using a time-series anomaly plot followed by correcting data to more reliable contemporaneous pH measurements. If and only if the reference pH is trustworthy, E^* is calculated such that the average anomaly between sensor and reference is minimized.

While these steps seem obvious now, we note that a number of sensor users have independently suggested applying a variety of corrections: forcing the sensor data to agree with every discrete sample (either through step or linear changes in E^*, despite lack of evidence to support such variability in E^*), attempting to correct uncorrectable (unconditioned, drifting, fouled, or faulty) data, or endeavoring to correct sensor data to bottle measurements of questionable quality.

3.6. Sensor redundancy

The DMB data provide a compelling reason to deploy multiple biogeochemical sensors. The availability of two reference electrodes, an oxygen sensor, and an empirical relationship between pH and O_2 allowed pH sensor data to be salvaged from the first deployment. Without the oxygen data, it would have been impossible to pinpoint the source of pH sensor drift between the ISFET, internal reference, and external reference electrodes. The drift in pH^{INT} relative to pH^{EXT} would have signaled a problem with the system and both pH values would have been flagged as 'bad'. This type of scenario is sometimes encountered by researchers who deploy a SeaFET with no additional co-located sensors. In these cases, the time-series anomaly of pH between the two independent reference electrodes is a useful tool, as it can help to identify sensor problems such as the onset of fouling.

Without independent validation based on bottle samples, additional sensors, or post-calibration, the output of any sensor must be skeptically viewed. Simply put, in a situation where a single pH electrode (ISFET, glass, etc.) is deployed with a single reference electrode in the absence of additional biogeochemical sensors or discrete samples to provide data QC, the resulting pH time-series should be viewed as unsubstantiated. We acknowledge that these requirements add complexity to sensor deployments but suggest that the returns in data quality are worth the effort. The Durafet sensor packages offer resolution that cannot practically be matched by discrete sampling programs and have gained popularity due to their ease of use and low cost. More complex and expensive systems may eventually provide pH data of higher quality that require less data QC, but it is doubtful that the

oceanographic community would accept data from any pH sensor as "climate quality" in the absence of independent validation.

In addition to pH and O_2, co-location of a third sensor for an additional CO_2 parameter provides an even more detailed approach to QC. Fig. 6(c) illustrates this, using the CCE-2 pH and pCO_2 sensor data. Due to the use of a measured carbonate parameter, (*viz.*, pCO_2) in $pH_{pCO_2}^{est}$, there is a discernibly tight relationship with sensor-based pH. Not surprisingly, the plot of sensor pH vs. $pH_{O_2}^{est}$ (Fig. 6(b)) exhibits greater scatter due to decoupling between oceanic O_2 and CO_2, likely as the result of the vastly different rates of O_2 and CO_2 air–sea gas exchange at the surface (Sarmiento and Gruber, 2006) or possibly due to variability in organismal CO_2:O_2 stoichiometry (Martz et al., 2014).

4. Conclusions

In this work we have shown that simple comparisons between contemporaneous measurements by biogeochemical sensors can reveal offset and drift in the sensors that would otherwise be undetectable. The nature and versatility of the QC approach employed depends on the number and type of co-located sensors and discrete samples. Actively flushed (i.e., pumped) sensor packages show far greater stability than passively flushed packages, with the former remaining stable in a wide variety of environments on timescales approaching one year, and the latter often succumbing to biofouling within one month. Below the euphotic zone, the flushing scheme appears to be less important, with both packages remaining stable for greater than nine months.

Two examples of successful operation of the Durafet sensor at depths of ∼90 m, slightly deeper than the rated tolerance of 100 psi, have been discussed. As more SeapHOx sensors are deployed below the mixed layer, the empirical equations relating pH and O_2 will surely provide an excellent backdrop for setting *in situ* calibration points and data QC. In turn, the sensors may provide insight into situations or locations where the empirical equations may not hold. We note that the Durafet sensor has recently been redesigned to operate at depths up to 2000 m and it is expected that the "Deep-Sea Durafet" will become commercially available in the future (Johnson et al., 2013).

It is shown that biofouling, rather than sensor drift or battery lifetime, often determines the timescale of usable data. In the worst cases, where passively flushed sensors were deployed in highly productive coastal environments, fouling compromised pH data within days to weeks (Fig. 5(b)). At the same location, the actively flushed SeapHOx exhibited no detectable drift over four months (Fig. 6(a)). Below the euphotic zone, however, the passively flushed SeaFET showed no sign of biofouling after more than 8 months (Fig. 2). Furthermore, biofouling appears to have a stronger temporal response than sensor drift. While a drifting internal reference electrode in the first DMB deployment causes an anomaly increase of ∼0.01 pHweek^{-1} (Fig. 5(c)), SeaFET biofouling at L20 is shown to increase the anomaly faster than 0.5 pHweek^{-1} (Fig. 5(b), Figure S1).

Best practices summary

1. Preceding deployment, operate sensors in natural seawater until initial sensor drift due to conditioning stops (approximately 5–10 days), with daily samples in order to observe the pre-deployment conditioning period; repeat this process following deployment for validation. Power the ISFET continuously during this period.
2. Best practices require a careful shore-side calibration point based on discrete sample(s) following the conditioning period.
3. Store sensors in seawater between deployments.
4. Prevent biofouling as permitted, especially within the euphotic zone.
    i. Utilize an actively flushed flow scheme that minimizes light.
    ii. Incorporate a Sea-Bird instrument with tributyltin plugs into the flow scheme.
    iii. Wrap sensor housings with tape (McMaster-Carr P/N 6029T98) and paint with EP-SN1 or similar antifouling paint.
    iv. When using passively flushed SeaFET sensors, incorporate a 70:30 Cu–Ni alloy tube into a flow stream around the Durafet and ISE.
5. When practical, take frequent discrete samples alongside a sensor throughout a deployment in order to establish an error estimate in the sensor data.

6. Deploy co-located, independent sensors such as redundant pH, pCO_2, and O_2 sensors.
7. Estimate pH from regional empirical (Alin et al., 2012) and/or thermodynamic relationships (e.g., CO2SYS.m; Van Heuven et al., 2011).
8. Assess and control pH^{sensor} data quality with pH^{disc} and pH^{est} using the following plots:
    i. *time-series anomaly* to first identify and then eliminate periods of ostensible sensor conditioning, drift, and failure.
    ii. *property–property* to examine agreement between pH^{sensor} and an independent reference pH (through the intercept, c_0, and slope, c_1). Property–property plots are useful for quality assessment; that is, a c_0 significantly different from 0 and/or c_1 from 1 indicates bias in the sensor and/or reference pH used for comparison.
9. Apply a single calibration point, chosen to minimize the anomaly relative to a trustworthy reference pH throughout the deployment. In particular, it is not recommended to force sensor data to agree with multiple individual bottle samples as this imparts sampling error to the sensor time series.
10. Establish an error envelope for the sensor time-series. The accuracy of the sensor time-series can be no better than the reference to which it is calibrated or validated (e.g., 0.024 when using $pH^{est}_{O_2}$ below the mixed layer in the region described by Alin et al. (2012), ~0.01 when using $pH^{est}_{pCO_2}$; uncertainty relative to discrete samples is estimated from the error of the anomaly time-series).

The contrast in conditions across multiple deployments has provided the opportunity to assess several important nuances in chemical sensor performance, leading to information that will help improve future data sets. While an outright sensor failure is easily detected, discerning the gradual effect of fouling or drift can be very difficult. Clearly, the combination of pH, pCO_2, and O_2 sensor data with the empirical equations provides a robust cross-check via the pH anomaly and property–property plots, allowing the QC analyst to detect the onset of subtle problems.

Acknowledgments

Appendix A. Supplementary data

The effects of biofouling are explored further in the attached Supplementary data. pH on the three most commonly reported scales is calculated as functions of the other two scales. Matlab code is provided for sensor calibration and calculation of pH from recorded voltages. Supplementary material related to this article can be found online at http://dx.doi.org/10.1016/j.mio.2014.08.003.

References

Alin, S.R., Feely, R.A., Dickson, A.G., Hernández-Ayón, J.M., Juranek, L.W., Ohman, M.D., Goericke, R., 2012. Robust empirical relationships for estimating the carbonate system in the southern California Current System and application to CalCOFI hydrographic cruise data (2005–2011). J. Geophys. Res. 117. http://dx.doi.org/10.1029/2011JC007511.

Bergveld, P., 2003. Thirty years of ISFETOLOGY: What happened in the past 30 years and what may happen in the next 30 years. Sensors Actuators B 88, 1–20. http://dx.doi.org/10.1016/S0925-4005(02)00301-5.

Byrne, R.H., Degrandpre, M.D., Short, R.T., Martz, T.R., Merlivat, L., McNeil, C., Sayles, F.L., Bell, R., Fietzek, P., 2009. Sensors and Systems for In Situ Observations of Marine Carbion Dioxide System Variables. OceanObs'09.

Clayton, T.D., Byrne, R.H., 1993. Spectrophotometric seawater pH measurements: total hydrogen ion concentration scale calibration of m-cresol purple and at-sea results. Deep Sea Res. Part I Oceanogr. Res. Pap. 40, 2115–2129. http://dx.doi.org/10.1016/0967-0637(93)90048-8.

Culberson, C., 1981. Direct potentiometry, in: Whitfield, M., Jagner, D. (Eds.), Marine Electrochemistry: A Practical Introduction. pp. 187–262.

Cullison Gray, S.E., DeGrandpre, M.D., Moore, T.S., Martz, T.R., Friederich, G.E., Johnson, K.S., 2011. Applications of in situ pH measurements for inorganic carbon calculations. Mar. Chem. 125, 82–90. http://dx.doi.org/10.1016/j.marchem.2011.02.005.

.A.G. Dickson, C.L. Sabine, and J.R. Christian (Eds.), 2007. Guide to Best Practices for Ocean CO2 Measurements, PICES Spec. ed.

Easley, R.A., Patsavas, M.C., Byrne, R.H., Liu, X., Feely, R.A., Mathis, J.T., 2013. Spectrophotometric measurement of calcium carbonate saturation states in seawater. Environ. Sci. Technol. 47, 1468–1477. http://dx.doi.org/10.1021/es303631g.

Emerson, S., Sabine, C., Cronin, M.F., Feely, R., Cullison Gray, S.E., DeGrandpre, M., 2011. Quantifying the flux of $CaCO_3$ and organic carbon from the surface ocean using in situ measurements of O_2, N_2, pCO_2, and pH. Global Biogeochem. Cycles 25, GB3008. http://dx.doi.org/10.1029/2010GB003924.

Friederich, G.E., Brewer, P.G., Herlien, R., Chavez, F.P., 1995. Measurement of sea surface partial pressure of $C0_2$ from a moored buoy. Deep Sea Res. Part I Oceanogr. Res. Pap. 42, 1175–1186. http://dx.doi.org/10.1016/0967-0637(95)00044-7.

Frieder, C.A., Nam, S.H., Martz, T.R., Levin, L.A., 2012. High temporal and spatial variability of dissolved oxygen and pH in a nearshore California kelp forest. Biogeosciences 9, 3917–3930. http://dx.doi.org/10.5194/bg-9-3917-2012.

Hofmann, G.E., Smith, J.E., Johnson, K.S., Send, U., Levin, L.A., Micheli, F., Paytan, A., Price, N.N., Peterson, B., Takeshita, Y., Matson, P.G., Derse Crook, E., Kroeker, K.J., Cristina Gambi, M., Rivest, E.B., Frieder, C.A., Yu, P.C., Martz, T.R., 2011. High-frequency dynamics of ocean pH: a multi-ecosystem comparison. PLoS One 6 http://dx.doi.org/10.1371/journal.pone.0028983.

Johnson, K.S., Jannasch, H.W., Coletti, L.J., Carlson, R., Brown, G., Nohava, T., Martz, T.R., Takeshita, Y., Swift, D., Riser, S.C., 2013. Towards a global ocean pH observing system: First observations with Deep-Sea Durafet pH sensors on profiling floats, in: ASLO Aquatic Sciences Meeting. New Orleans, LA.

Khoo, K.H., Ramette, R.W., Culberson, C.H., Bates, R.G., 1977. Determination of hydrogen ion concentrations in seawater from 5 to 40°C: standard potentials at salinities from 20 to 45 per mil. Anal. Chem. 49, 29–34. http://dx.doi.org/10.1021/ac50009a016.

Kline, D.I., Teneva, L., Schneider, K., Miard, T., Chai, A., Marker, M., Headley, K., Opdyke, B., Nash, M., Valetich, M., Caves, J.K., Russell, B.D., Connell, S.D., Kirkwood, B.J., Brewer, P., Peltzer, E., Silverman, J., Caldeira, K., Dunbar, R.B., Koseff, J.R., Monismith, S.G., Mitchell, B.G., Dove, S., Hoegh-Guldberg, O., 2012. A short-term in situ CO_2 enrichment experiment on Heron Island (GBR). Sci. Rep. 2, 413. http://dx.doi.org/10.1038/srep00413.

Liu, X., Patsavas, M.C., Byrne, R.H., 2011. Purification and characterization of meta-cresol purple for spectrophotometric seawater pH measurements. Environ. Sci. Technol. 45, 4862–4868. http://dx.doi.org/10.1021/es200665d.

Liu, X., Wang, Z.A., Byrne, R.H., Kaltenbacher, E.A., Bernstein, R.E., 2006. Spectrophotometric measurements of pH in-situ: laboratory and field evaluations of instrumental performance. Environ. Sci. Technol. 40, 5036–5044. http://dx.doi.org/10.1021/es0601843.

Marion, G.M., Millero, F.J., Camões, M.F., Spitzer, P., Feistel, R., Chen, C.-T.A., 2011. pH of seawater. Mar. Chem. 126, 89–96. http://dx.doi.org/10.1016/j.marchem.2011.04.002.

Martz, T.R., Connery, J.G., Johnson, K.S., 2010. Testing the honeywell durafet for seawater pH applications. Limnol. Oceanogr. Methods 8, 172–184. http://dx.doi.org/10.4319/lom.2010.8.172.

Martz, T.R., Send, U., Ohman, M.D., Takeshita, Y., Bresnahan, P.J., Kim, H.-J., Nam, S., 2014. Dynamic variability of biogeochemical ratios in the Southern California current system. Geophys. Res. Lett. 41, 2496–2501. http://dx.doi.org/10.1002/2014GL059332.

Peltzer, E., 2007. Model II least squares fit: lsqfitma.m, http://www.mbari.org/staff/etp3/regress/lsqfitma.m.

Riebesell, U., Fabry, V.J., Hansson, L., Gattuso, J.-P. (Eds.), 2010. Guide to Best Practices for Ocean Acidification Research and Data Reporting. Publications Office of the European Union, Luxembourg.

Sarmiento, J.L., Gruber, N., 2006. Ocean Biogeochemical Dynamics. Princeton University Press, Princeton, NJ.

Seidel, M.P., DeGrandpre, M.D., Dickson, A.G., 2008. A sensor for in situ indicator-based measurements of seawater pH. Mar. Chem. 109, 18–28. http://dx.doi.org/10.1016/j.marchem.2007.11.013.

Takeshita, Y., Martz, T.R., Johnson, K.S., Dickson, A.G., Characterization of an ion sensitive field effect transistor and chloride ion selective electrodes for pH measurements in seawater, Anal. Chem. (submitted for publication).

Van Heuven, S., Pierrot, D., Rae, J.W.B., Lewis, E., Wallace, D.W.R., 2011. MATLAB Program Developed for CO_2 System Calculations. http://dx.doi.org/10.3334/CDIAC/otg.CO2SYS_MATLAB_v1.1.

Yu, P.C., Matson, P.G., Martz, T.R., Hofmann, G.E., 2011. The ocean acidification seascape and its relationship to the performance of calcifying marine invertebrates: Laboratory experiments on the development of urchin larvae framed by environmentally-relevant pCO_2/pH. J. Exp. Mar. Bio. Ecol. 400, 288–295. http://dx.doi.org/10.1016/j.jembe.2011.02.016.